

Induction of apoptosis in Ehrlich ascites tumour cells via p53 activation by a novel small-molecule MDM2 inhibitor – LQFM030

Mariana F. da Mota^{a,b}, Alane P. Cortez^a, Polyana L. Benfica^a, Bruna dos S. Rodrigues^a, Thalyta F. Castro^a, Larissa M. Macedo^c, Carlos H. Castro^c, Luciano M. Lião^d, Flávio S. de Carvalho^{d,f}, Luiz A. S. Romeiro^e, Ricardo Menegatti^f, Hugo Verli^g, Bianca Villavicencio^g and Marize C. Valadares^{a*}

^aLaboratório de Farmacologia e Toxicologia Celular, FarmaTec, Faculdade de Farmácia, Universidade Federal de Goiás, UFG, Goiânia, GO, Brazil

^bLab. de Biologia e DNA Forense da Polícia Técnico-Científica de Goiás, GO - Brazil, Universidade Federal de Goiás, UFG, Goiânia, GO, Brazil,

^cDepartamento de Fisiologia e Farmacologia, Instituto de Ciências Biológicas, Universidade Federal de Goiás, UFG, Goiânia, GO, Brazil, ^dInstituto de Química, Universidade Federal de Goiás, UFG, Goiânia, GO, Brazil, ^eFaculdade de Ciências da Saúde, Universidade de Brasília, UNB, Brasília, DF, Brazil,

^fLaboratório de Química Farmacêutica Medicinal (LQFM), Faculdade de Farmácia, Universidade Federal de Goiás, UFG, Goiânia, GO, Brazil

and ^gCentro de Biotecnologia, Universidade Federal de Rio Grande do Sul, UFRS, Porto Alegre, RS, Brazil

Keywords

Ehrlich ascites tumor; LQFM030; MDM2; Nutlins; p53

Correspondence

Marize C. Valadares, Laboratório de Farmacologia e Toxicologia Celular, Faculdade de Farmácia, Universidade Federal de Goiás, Praça Universitária 1166, 74605 220 Goiânia, GO, Brazil.
E-mail: marizecv@ufg.br

Received October 1, 2015

Accepted April 30, 2016

doi: 10.1111/jphp.12573

Abstract

Objective The activation of the p53 pathway through the inhibition of MDM2 has been proposed as a novel therapeutic strategy against tumours. A series of cis-imidazoline analogues, termed nutlins, were reported to displace the recombinant p53 protein from its complex with MDM2 by binding to MDM2 in the p53 pocket, and exhibited an antitumour activity both *in vitro* and *in vivo*. Thus, the purpose of this study was to evaluate the antitumour properties of LQFM030 (2), a nutlin analogue created by employing the strategy of molecular simplification.

Methods LQFM030 (2) cytotoxicity was evaluated in Ehrlich ascites tumour (EAT) cells, p53 wild type, by the trypan blue exclusion test, and the mechanisms involved in EAT cell death were investigated by light and fluorescence microscopy, flow cytometry, real-time PCR and Western blotting.

Key findings Our results demonstrate that LQFM030 has dose-dependent antiproliferative activity and cytotoxic activity on EAT cells, induces the accumulation of p53 protein and promotes cell cycle arrest and apoptosis. p53 gene transcription was unaffected by LQFM030 (2); however, MDM2 mRNA increased and MDM2 protein decreased.

Conclusions These results suggest that the small-molecule p53 activator LQFM030 (2) has the potential for further development as a novel cancer therapeutic agent.

Introduction

The activation of the p53 pathway via the inhibition of MDM2 has been proposed as a novel therapeutic strategy. In fact, studies have shown that the disruption of the p53–MDM2 interaction by different macromolecular approaches or by the suppression of MDM2 expression can lead to the activation of p53 and tumour growth inhibition.^[1–3]

p53 is an important defence against cancer because it controls the transition of cells from the G1 to S phase and also induces cell cycle arrest and apoptosis.^[4,5] Due to its

potent tumour suppressor role, the p53 pathway is usually altered in tumour cells. Indeed, inactivating mutations in p53 gene are found in approximately 50% of all human cancers; in the remaining cancers in which the p53 is not mutated, the function of the p53 pathway is often inhibited via other mechanisms, including the increased expression of MDM2 (a negative regulator of p53). The fact that the p53 signalling pathway is inactivated in virtually all cancers has drawn great attention from the worldwide cancer research community for targeting the p53 pathway for the development of improved cancer therapies.^[2] Thus,

drugging p53 pathway through the disruption of the p53–MDM2 interaction using non-peptide small-molecule inhibitors has recently appeared as an effective therapeutic strategy for different tumours. Actually, several MDM2 inhibitors are described in the literature presenting different structures, dihydroimidazothiazoles, oxopiperidine, imidazoles and oxomorpholins, and many of them reached already clinical trials.^[3]

Nutlins (a series of cis-imidazoline analogues) are currently considered among the most promising activators of p53 to induce p53-dependent apoptosis in several tumour cells.^[6–8] Nutlins bind tightly into the p53 pocket of MDM2, activate p53 pathway and trigger apoptosis in wild-type p53 tumour cells.^[6,9]

In view of the potential antitumour property of nutlins and its complex, analogues of this compound have been designed to optimize the complex production and maintain the antitumour activity and apoptosis-inducing activity. One such analogue is LQFM030 (2), a heterocyclic compound originally based on the prototype nutlin-1 using molecular simplification (Figure 1a). This compound was designed and synthesized by our group, and previous studies demonstrated that LQFM030 (2) has a significant cytotoxicity and apoptosis-inducing potential against a human leukaemic cell line. Changes in cell cycle progression, increasing Bax and decreasing Bcl-2 expression, cytochrome c release and loss of the mitochondrial membrane potential were observed with this compound. Furthermore, the compound increased the survival of tumour-bearing mice and showed low toxicity (unpublished data).

Considering that Ehrlich ascites tumour (EAT) is originally a carcinoma with wild-type p53 cell,^[10–12] the aim of the current study was to examine the antitumoral activity and the cell death mechanisms triggered by the novel synthetic MDM2 inhibitor LQFM030 (2) on EAT cells through the disruption of the p53–MDM2 complex.

Materials and Methods

Chemicals and antibodies

RPMI-1640 medium, fetal bovine serum, streptomycin, penicillin G, propidium iodide and RNase were purchased from Sigma Aldrich (St. Louis, MO, USA). Ethanol, trypan blue and Tween 20 were obtained from Vetec (Rio de Janeiro, RJ, Brazil). Hoechst 33342 and the BCIP/NBT substrate kit were acquired from Invitrogen/Life Technologies (Carlsbad, CA, USA). Cytofix/Cytoperm was obtained from BD Biosciences (San Jose, CA, USA). The Annexin V apoptosis detection FITC kit was obtained from eBioscience (San Diego, CA, USA). The CaspaTag Caspase *In Situ* Assay Fluorescein kit (caspases-3/7, -8 and -9) was purchased from Millipore Corporation (Billerica, MA, USA). TRIzol

was obtained from Life Technologies (Carlsbad, CA, USA). The RNeasy mini kit, QuantiTect Reverse Transcription kit and Qiagen Rotor-Gene SYBR Green PCR kit were acquired from Qiagen (Valencia, CA, USA). NP-40 lysis buffer and protease inhibitor cocktail were from Amresco (Solon, OH, USA). All antibodies used were purchased from Santa Cruz Biotechnologies (Santa Cruz, CA, USA).

LQFM030 (2) synthesis

Synthesis of 1-(4-((1-(4-chlorophenyl)-1H-pyrazol-4-yl)methyl) piperazin-1-yl) ethanone (2)

To a 500-ml round-bottomed flask, 9.67 mmol of 1-(4-chlorophenyl)-1H-pyrazole-4-carbaldehyde (5), 10.64 mmol of acetyl piperazine (6), 100 mg of Pd/C 10%, 70 ml of methanol and 60 psi of H₂ were added. The resulting solution was filtered, and compound (2) was obtained as a beige solid; the quantitative yield was mp 92°C, R_f = 0.56 (CH₂Cl₂:MeOH – 95:5). IR cm⁻¹: 3010, 2947, 1639 and 830. ¹HNMR: (500 MHz, CDCl₃) δ 7.83 (d, *J* = 0.6 Hz, H-5), 7.64 (d, *J* = 0.6 Hz, H-3), 7.62 (dd, *J* = 9.8, 2.2 Hz, H-2'), 7.62 (dd, *J* = 9.0, 2.2 Hz, H-6'), 7.41 (dd, *J* = 9.0, 3.0 Hz, H-3'), 7.41 (dd, *J* = 9.0, 2.9 Hz, H-5'), 3.63 (dd, *J* = 6.0, 4.0 Hz, H-11), 3.50 (s, H-6), 3.47 (dd, *J* = 6.0, 4.0 Hz, H-9), 2.47 (dd, *J* = 6.0, 4.0 Hz, H-12), 2.45 (dd, *J* = 6.0, 4.0 Hz, H-8) ppm and 2.08 (s, H-14). ¹³CNMR (125 MHz, CDCl₃) δ 168.8 (C-13), 141.9 (C-3), 138.6 (C-1'), 131.9 (C-4'), 129.6 (C-3'/C-5'), 126.4 (C-5), 119.9 (C-2'/C-6'), 119.6 (C-4), 52.7 (C-12), 52.3 (C-8), 52.2 (C-6), 46.2 (C-9), 41.5 (C-11) and 21.3 (C-14) ppm. LC-MS with electrospray ionization: *m/z* 319.16 [M + H]⁺.

A colourless needle-shaped single crystal of (I) with dimensions 0.075 × 0.16 × 0.47 mm was mounted on a Bruker Apex II Duo diffractometer, operating with Mo-K α radiation and at room temperature. Data collection was performed using φ/ω scans of 0.5° steps and exposure times of 20 s. Data reduction was carried out using SAINT and SADABS,^[13] employing the multiscan absorption correction method. The structure solution was accomplished with the direct methods followed by the refinement of structural parameters using *F*² with the full-matrix least-squares method; both methods are implemented in the Shelx software package.^[14] Non-hydrogen atoms were refined with anisotropic atomic displacement parameters, and the hydrogen atoms were treated as isotropic and were allowed to depend on their parent atoms with $U_{eq} = 1.2 U_{eq}(C_{aromatic}, CH_2)$ and $1.5 U_{eq}(C_{methyl}, O_{water})$. Hydrogen atoms were located in calculated positions, and the hydrogen atoms of the structural water molecule were located in the Fourier difference map and restrained with O–H distance of 0.92 Å. Infrared (IR) spectra were obtained with a Nicolet-55a Magna spectrophotometer using potassium bromide plates. The assays were carried out using LC-

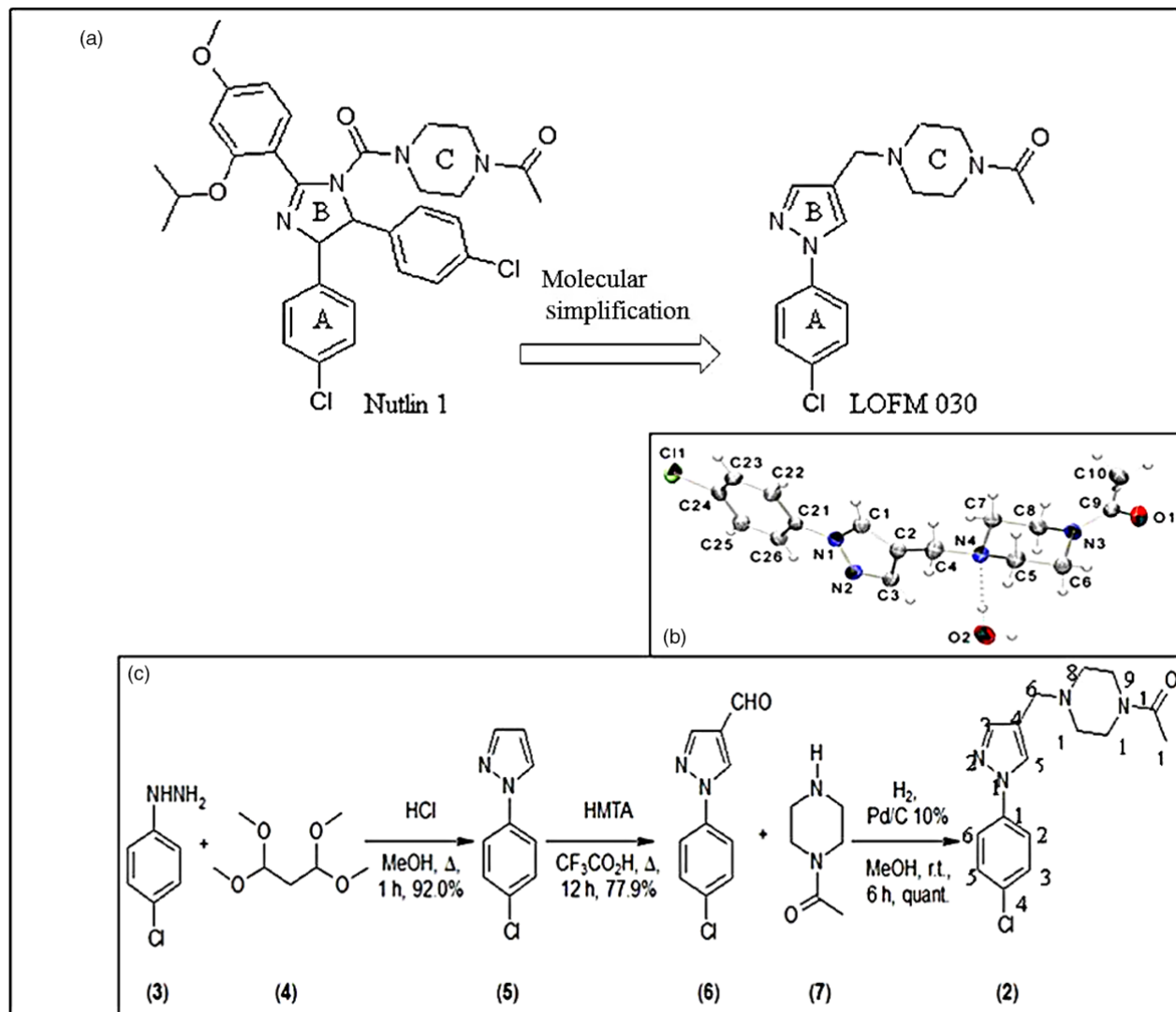


Figure 1 (a) Design of LQFM030 (**2**) from nutlin (**1**). (b) Ortep representation of LQFM030 (**2**) with atomic displacement parameters drawn at 30% of probability level. Hydrogens are represented by spheres of arbitrary radii. (c) Synthetic route of LQFM030 (**2**).

ESI-MS/MS mass spectrometer equipped with electrospray ionization source in the positive mode, ESI (Agilent Technologies 1200 Series/Applied Biosystems MDS Sciex API 3200 Triple Quadrupole, MS/MS, Santa Clara, CA, USA). The progress of all the reactions was monitored by thin-layer chromatography (TLC), which was performed on 2.0- to 6.0-cm aluminium sheets precoated with silica gel 7 60 (Merck, Kenilworth, NJ, USA) to a thickness of 0.25 mm. The developed chromatograms were viewed under ultraviolet light (254–265 nm) and treated with iodine vapour. For column chromatography, we used Merck silica gel (70–230 mesh). Reagents and solvents were purchased from commercial suppliers.

CCDC number 963584 contains the supplementary crystallographic data for compound (**2**). These data can be

obtained free of charge via <http://www.ccdc.cam.ac.uk/conts/retrieving.html> or from the Cambridge Crystallographic Data Centre, 12 Union Road, Cambridge CB21EZ, UK; fax: (+44) 1223-336-033; or e-mail: deposit@ccdc.cam.ac.uk.

The compound LQFM030 (**2**) was stored in a freezer at -20°C and prepared in the form of an oil/water emulsion at the time of testing, due to its hydrophobicity. The emulsion was prepared as follows. A sample of 5 mg/ml of LQFM030 (**2**) was added to 100 μl sunflower oil, 100 μg soya phosphatidylcholine and 50 μl ethanol. The mixture was vortexed for 3 min, and the final volume was completed with ultrapure water. For the control group, the emulsion was prepared without LQFM030 (**2**).

Molecular docking

Based on the crystallographic structure of MDM2 complexed with nutlin-3a (PDB ID 4HG7),^[15] we built LQFM030 in Avogadro^[16] and calculated partial charges with CHELPG^[17] using GAMESS.^[18,19] The receptor MDM2 and the ligands nutlin-3a and LQFM030 were prepared for docking using AutoDockTools4^[20,21] and then submitted for docking using DockThor^[22,23] and Auto-dock.^[24] The best resulting pose of each docking program was compared with nutlin-3a and P53 complexed with MDM2 using PyMol (The PyMOL Molecular Graphics System, version 1.7.4, Schrodinger Inc., New York, NY, USA), and contacts were detected with LigPlot+.^[25]

Mice

Male Swiss albino mice (25–30 g) were obtained from Industria Química do Estado de Goiás, Goiania, GO, Brazil. All of the animals were kept under constant environmental conditions, with a 12-h/12-h light–dark cycle and temperature of $23 \pm 2^\circ\text{C}$, fed standard granulated chow and given drinking water *ad libitum*. The animal experiments were performed in accordance with the Institutional Protocols of Animal Care. The experimental protocol (CEUA – PRPPG/UFG no. 018/12) was approved by Institutional Ethic Committee of this university.

Cell culture, growth conditions and treatment

EAT was maintained in Swiss albino mice in ascites form by successive transplantations. Ascitic tumour cell counts were made in a Neubauer haemocytometer using the trypan blue dye exclusion method. Cell viability was always found to be 95% or more. Tumour cell suspensions were prepared in phosphate-buffered saline solution (PBS) at pH 7.4 to final concentrations of 6×10^7 viable cells/ml.

Ten days after the inoculation of EAT cells in the abdominal cavity of mice, the cells were isolated by needle aspiration, washed in saline and cultured in RPMI 1640 supplemented with HEPES (25 mM), L-glutamine (2 mM), sodium bicarbonate (25 mM), 10% FBS, 2-mercaptoethanol (50 μM) and antibiotics (100 U/ml penicillin and 100 $\mu\text{g}/\text{ml}$ streptomycin). The cells were incubated in culture flasks at 37°C in a humidity atmosphere containing 5% of CO_2 .

Assessment of cell viability by the trypan blue exclusion method

EAT cells (5×10^5 cells/ml) were seeded into 96-well flat-bottomed microtitre plates (TPP, Trasadingen, Switzerland) in RPMI-1640 medium supplemented with 10% FBS and

incubated with or without eight concentrations (0.033–4.320 mM) of LQFM030 in sextuplicate for 24 or 48 h. The cell suspension and a trypan blue solution (0.2% in phosphate-buffered saline (PBS)) were mixed 1 : 10, and the viability of the cells was estimated using a haemocytometer (Boeco, Hamburg, Germany); the stained cells were scored as dead.

Morphological analysis by light and fluorescence microscopy

EAT cells were treated with LQFM030 (2) with 810 μM and incubated for 24 h, cytopinned onto glass slides and stained with HE. After staining, the slides were examined using light microscopy (Axio Scope.A1 Carl Zeiss®, Oberkochen, Germany), and the images were captured using a 100 \times objective with the AxioVs40 software, 4.7.2.0, Carl Zeiss, Oberkochen, Germany. The nuclear alterations were assessed using the DNA-binding dye Hoechst 33342, as described,^[26] using a 20 \times objective.

DNA cell cycle analysis

For the determination of the cell cycle-phase distribution and cell proliferation, 5×10^5 EAT cells/ml were incubated with or without 810 μM LQFM030 (2) for 24 h. The cells were washed twice with PBS at 1500 rpm for 10 min, and the cell pellets were resuspended in ice-cold 70% ethanol overnight at 4°C . The suspension was centrifuged, and the cell pellet was resuspended in 500 μl PBS solution containing 0.2 mg/ml RNase and 0.05 mg/ml PI and incubated at 4°C for 2 h. Fluorescence was measured with the FACS-Canto II flow cytometer (BD Biosciences) using PE x FL2 channels. The assay was performed in triplicate, and 10 000 events were acquired. The analysis of the data was performed using ModFit software, BD Bioscience, San Jose, CA, USA.

Detection of apoptosis by an Annexin V binding assay

PS externalization was analysed by flow cytometry using the Annexin V apoptosis detection FITC kit. Cells (1×10^6 cells/ml) untreated and treated with 810 μM LQFM030 (2) for 24 h were washed with PBS and resuspended in 0.1 ml of the binding buffer. The cells were stained with an anti-Annexin V-FITC antibody and propidium iodide (PI), following the manufacturer's instructions, and scanned in the FL-1 (FITC) vs. FL-2 (PI) channels.

Flow cytometric determination of cell membrane integrity

For the determination of cell membrane integrity, EAT cells (1×10^6 cells/ml) untreated and treated with 810 μM

LQFM030 (2) for 24 h were washed with PBS and incubated for 5 min in a solution of PI (2 µg/ml) in PBS. A total of 10 000 events were acquired for the analysis using the FACS Diva software, BD Bioscience, San Jose, CA, USA and a histogram plot of the PE fluorescence (*x*-axis) versus counts (*y*-axis) was shown as the logarithmic fluorescence intensity.

Flow cytometric analysis of DNA fragmentation

The amount of fragmented DNA was measured by flow cytometry. EAT cells (1×10^6 cells/ml) untreated and treated with 810 µM LQFM030 (2) for 24 h were washed with PBS and incubated with 0.2 ml lysis buffer (0.1% sodium citrate, 0.1% Triton X-100 and 2 µg/ml PI) for 15 min at 4°C. A total of 10 000 events were acquired for the analysis using the FACS Diva software, and a histogram plot of the PE fluorescence (*x*-axis) versus counts (*y*-axis) was shown as the logarithmic fluorescence intensity.

Flow cytometric analysis of the protein expression of p53, p21 and p27

For the determination of the expression of the pro-apoptotic proteins p53, p21 and p27, EAT cells (1×10^6 cells/ml) untreated and treated with 810 µM LQFM030 (2) for 24 h were washed with PBS, suspended in 0.25 ml of a fixation and permeabilization solution (Cytotfix/Cytoperm) and incubated for 20 min at 4°C. The cells were then washed twice in PBS-T20 and incubated with specific antibodies (anti-p53, anti-p21 or anti-p27) for 15 min at room temperature. The cells were washed in PBS-T20. A total of 10 000 events were acquired for the analysis using the FACS Diva software, and a histogram plot of the FITC or PE fluorescence (*x*-axis) versus counts (*y*-axis) was shown as the logarithmic fluorescence intensity.

Quantitative RT-PCR

Transcriptional profile of p53, MDM2, p21, caspases-3, -8 and -9 was analysed after the treatment of EAT cells with 405 µM LQFM030 (2). Total RNA from EAT cells was obtained using the TRIzol reagent or the RNeasy mini kit, following the manufacturers' instructions. Concentration and the purity of the isolated RNA were determined by measuring the optical density at 260 and 280 nm (Nano-Drop 8000 – Thermo Scientific, Waltham, MA, USA). The RNA integrity was verified by electrophoresis through 1.5% agarose gels stained with ethidium bromide. QuantiTect Reverse Transcription Kit (Qiagen) was used for cDNA synthesis with 1 µg of RNA, following the manufacturer's instructions. Real-time PCR was performed with 2 µl of

cDNA diluted 1/10 and 200 nM of primers using Rotor-Gene SYBR Green PCR kit (Qiagen). All experiments were run with controls NTC and -RT. PCR specificity was determined using both a melting curve analysis and gel electrophoresis.

The sequences of primers were described for p53 and p21,^[27] caspase-3, -8, -9^[28] and PGK1 (phosphoglycerate kinase 1).^[29] MDM2 primers were constructed using Primer3 and BLAST (NCBI): forward 5'-TCCCCTTATCGTC TGGGAAGC-3'; reverse: 5'-GAGATTTCTTAGCTGACTA TTGG-3'. PCR conditions were as follows: 95°C for 5 min, followed by 40 cycles of 5 s for 95°C and 10 s at 60°C using Rotor-Gene (Qiagen) equipment. The endogenous gene used for normalization was PGK1. The relative expression was calculated using the $2^{-\Delta\Delta C_t}$ method.^[30] The results were obtained from two independent experiments; each was carried out in duplicate and repeated three times.

Western blot analysis of MDM2

For the Western blot analysis of the MDM2 protein, EAT cells (5×10^5 cells/ml) were treated or untreated with 810 µM LQFM030 (2), and the cell lysates were prepared with NP-40 lysis buffer (containing a protease inhibitor cocktail) for 30 min on ice. The cell debris was pelleted by centrifugation at 2200 g and 4°C for 10 min, and the supernatant was recovered. Approximately 40 µg of protein, as estimated by the Bradford method, was separated on a 10% SDS-polyacrylamide gel and electrotransferred to nitrocellulose membranes (Millipore). After blocking with 5% non-fat skim milk powder in BSA, the membranes were incubated with an antibody against MDM2 (1 : 250). The blots were washed three times with TBST and incubated with the secondary antibody tagged with alkaline phosphatase (1 : 1000) for 1.5 h. After washing with TBST for 30 min, the MDM2 protein was detected using the chromogenic substrate BCIP/NBT. Equal protein loading in each lane was confirmed by probing with an anti-GAPDH antibody (1 : 1000). Quantification of the band density was performed using ImageJ software and calculated as the ratio of GAPDH expressed in the same sample.

Flow cytometric analysis of caspases-3/7, -8 and -9 expression

The activity of caspases-3/7, -8 and -9 was measured using the CaspaTag Caspase *In Situ* Assay Fluorescein kit following the manufacturer's instructions. A total of 10 000 events were acquired for the analysis using the FACS Diva software, and a histogram plot of the FITC fluorescence (*x*-axis) versus counts (*y*-axis) was shown as the logarithmic fluorescence intensity.

Statistical analysis

The data were represented as the mean \pm SD, and the values were obtained in at least two independent experiments repeated three times each (n). The statistical analyses were performed using Student's t -test with the GraphPad Prism program (GraphPad Software version 5.0; San Diego, CA, USA). Differences were considered significant when P -values were <0.05 .

Results

LQFM030 (2) synthesis

LQFM030 (2) was produced via the synthetic route shown in Figure 1, beginning with synthesis of the 1-(4-chlorophenyl)-1*H*-pyrazole (4) compound using the classical method described by,^[13] with a yield of 92.0%. The 1-(4-chlorophenyl)-1*H*-pyrazole-4-carbaldehyde (4) compound was produced (with a yield of 77.9%) via chemospecific and region-specific formulation of 1-(4-chlorophenyl)-1*H*-pyrazole (5), which was performed under Duff's conditions.^[14] LQFM030 (2) was obtained under catalytic hydrogenation conditions with a quantitative yield. After three steps, LQFM030 (2) was produced with a global yield of 71.6%, which was higher than that of the compound nutlin 1 (1), which was produced with a global yield of 6.4% in eight synthetic.^[31]

The structure of the compounds was investigated and confirmed by infrared spectroscopy and NMR spectroscopy, combining the ¹H, HSQC and HMBC correlation spectra, as well as mass spectrometry.

X-ray analysis

An Ortep representation of LQFM030 (2) is given in Figure 1b and shows a staggered conformation in which the chlorophenyl ring is at a dihedral angle of 10.5 (1)° to the pyrazole ring. The C4 atom is located 0.133 (3) Å from the best plane of the pyrazole. The piperazine presents a chair conformation with the best plane (of r.m.s. of 0.004 Å) of the carbon atoms C5/C6/C7/C8 rotated 70.14 (7)° from the pyrazole plane. The N4 atom has sp³ hybridization, while the N3 atom is sp², with a N3–C9 bond distance of 1.345 (3) Å and the other N–C bond lengths varying from 1.459 (2) to 1.473 (2) Å. As a consequence of the N3sp³ hybridization, the formyl group C9/C10/O1 is in a plane (r.m.s. 0.005 Å) with the atoms C6/N3/C8.

LQFM030 (2) was obtained as a monohydrate chiral crystalline solid, indicating that the present conformation is stable under normal conditions and showing the strong affinity of the piperazine N atom for a proton donor. The water molecule participates in two strong hydrogen bonds

with (1). As suggested by the short donor acceptor (DA) distance of 2.917 (2) Å and the linearity of the O2–H...N4 H-bond with an angle of 169 (3)°, this water molecule connects neighbour molecules (symmetry operation $i: x - 1/2, -y + 1/2, -z + 1$) with a H-bond of type O2–H...O1ⁱ, a DA distance of 2.816 (2) Å and a OHO angle of 171 (2)° (Table 1). The structure of LQFM030 (2) determined using X-ray diffraction is illustrated in Figure 1b.

Molecular Docking studies

Docking analysis revealed that the chlorophenyl group of LQFM030 (2) calculated by Autodock is located in proximity of the same group of nutlin-3a, and so is Trp23 of P53 (Figure 2). The same group of LQFM030 (2) calculated by DockThor is close to the other chlorophenyl group of nutlin-3a, being close to Leu26 of P53, which is also an important residue in interaction with MDM2.^[32]

LQFM030 (2) induced cytotoxicity in EAT cells

The effects of LQFM030 (2) on the viability of EAT cells using the trypan blue exclusion test were investigated. EAT cells were treated with LQFM030 (2) at increasing concentrations (0.033–4.32 mM). A marked concentration-dependent growth inhibition was observed when the cells were treated with LQFM030 (2) for 24 and 48 h. LQFM030 (2) showed 50% growth inhibition after 24 h of treatment at 810 μM; the IC₅₀ value was 100 μM after 48 h of treatment (Figure 3a). Using the IC₅₀ value for 24 h (810 μM), we detected a loss of plasma membrane integrity in 27.25 \pm 2.1% of the EAT cells by flow cytometry after incubation with PI (Figure 3b).

Table 1 Data collection and refinement statistics

LQFM030 (I)	
Data collection	
Space group	P2 ₁ 2 ₁ 2 ₁
Cell dimensions	
<i>a</i> , <i>b</i> , <i>c</i> (Å)	6.0320 (8), 8.9792 (13), 31.306 (5)
Resolution (Å)/θ interval (°)	0.8/1.30–26.28
<i>R</i> _{symm} / <i>R</i> _{int}	0.022/0.017
//σ _i	1.86
Completeness (%)	99.7
Redundancy	4.36
Refinement	
Resolution (Å)	0.8
No. reflections total/ <i>l</i> > 2σ _{<i>i</i>}	12 724/3406
<i>R</i> ₁ / <i>wR</i> ₂ (all data)	0.044/0.087
No. parameters/restraints	217/3
R.m.s. deviations	
Bond lengths (Å)	0.003
Bond angles (°)	0.20

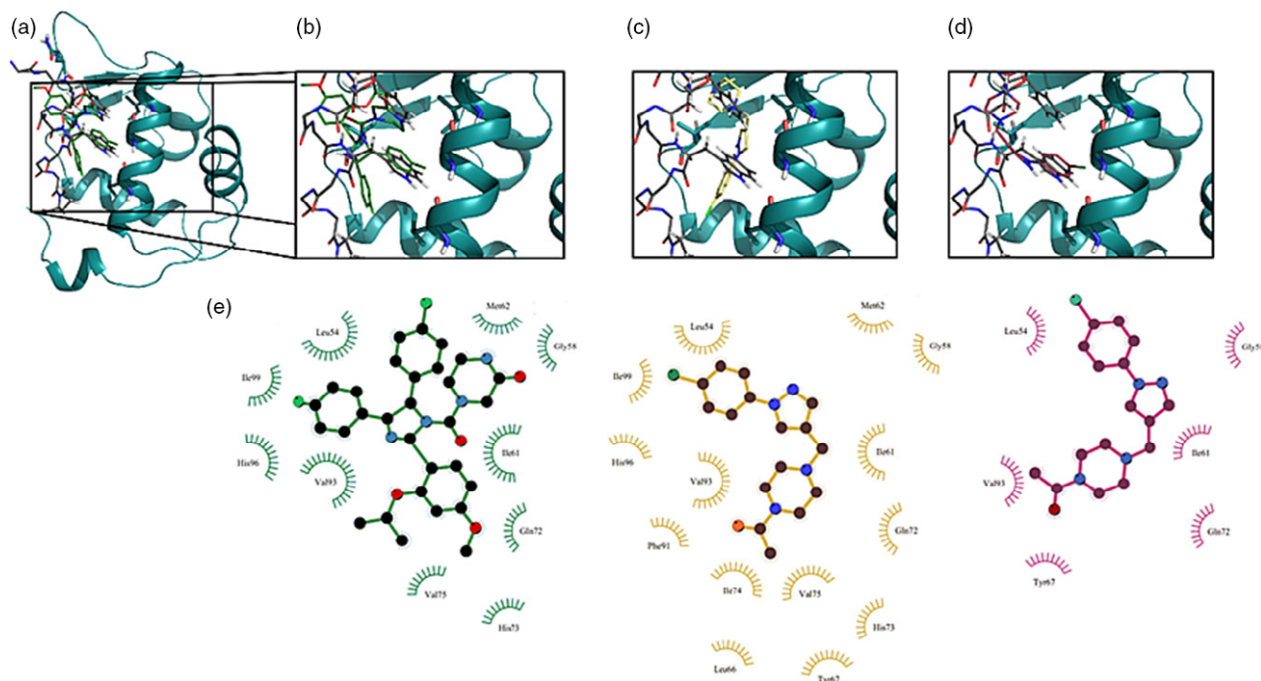


Figure 2 Interaction of ligands with MDM2. (a) General view of MDM2 (teal) complexed with P53 (grey) and nutlin-3a (green). (b) Detail of the superposition of an aromatic ring with chlorine from nutlin-3a and a tryptophan of P53, which is a key residue in the interaction of P53 with MDM2. (c) Interaction between P53 and LQFM030 as calculated by DockThor. (d) Interaction between P53 and LQFM030 as calculated by Autodock (notice the superposition of the aromatic ring with chlorine of LQFM030 and the tryptophan of P53). (e) Hydrophobic contacts of MDM2 with nutlin-3a and with LQFM030 by DockThor and Autodock, respectively. Notice the recurrence of Gly58, Ile61, Gln72 and Val93, which also interact with P53 (not shown), and Leu54, which interacts with tryptophan from P53.

LQFM030 promoted morphological and nuclear changes in EAT cells

The morphological analysis of EAT cells stained with HE clearly revealed the presence of apoptotic cells after the treatment with LQFM030 (2). As can be observed in Figure 4a, the control cells exhibited nuclei with dispersed chromatin and an organized plasma membrane. In contrast, the cells treated with LQFM030 (2) for 24 h presented membrane blebbing, vacuolization (Figure 4b) and nuclear fragmentation (Figure 4c). After nuclear staining with Hoechst 33342, the nuclei in the viable cells displayed a regular, oval shape, with homogeneous chromatin (Figure 4d), whereas shrinking and fragmentation of the nuclei, chromatin condensation and low fluorescence were observed in the apoptotic cells (Figure 4e).

LQFM030 promoted cell cycle arrest in EAT cells

To evaluate whether LQFM030 (2) treatment of EAT cells would interfere in cell cycle dynamics, cytometry analyses were performed. The results revealed that LQFM030 (2) treatment significantly arrested the EAT cells at the G1

phase. There was a meaningful increase in the cells in G1 phase ($74.79 \pm 8.9\%$) compared with the untreated cells ($45.80 \pm 6.6\%$; $P < 0.05$), while cells in S phase ($15.15 \pm 5.9\%$) decreased. Although there was no statistical relevance, G2/M phase arrest also could be detected (Figure 5). These data suggest that LQFM030 (2) could arrest the cell cycle at G1 and G2/M and prevent EAT cell proliferation.

LQFM030 (2) induced phosphatidylserine externalization and DNA fragmentation on EAT cells

To further explore the EAT cell death mechanisms triggered by LQFM030 (2) and whether it elicits similar apoptosis, phosphatidylserine (PS) exposure was assessed using Annexin V/PI double staining (Figure 6a–c). Although phosphatidylserine exposure does not occur in all apoptosis cases,^[33,34] this process is frequently used to evaluate the apoptotic cell death. As determined by the cytometric analysis, a reduction in viable cells was observed after LQFM030 (2) treatment (90.45 to $54.20 \pm 1.1\%$; $P < 0.05$), with an increase of $15.35 \pm 0.9\%$ of early apoptotic cells (Annexin V +/PI –; $P < 0.05$) and $12.80 \pm 0.28\%$ of late apoptotic

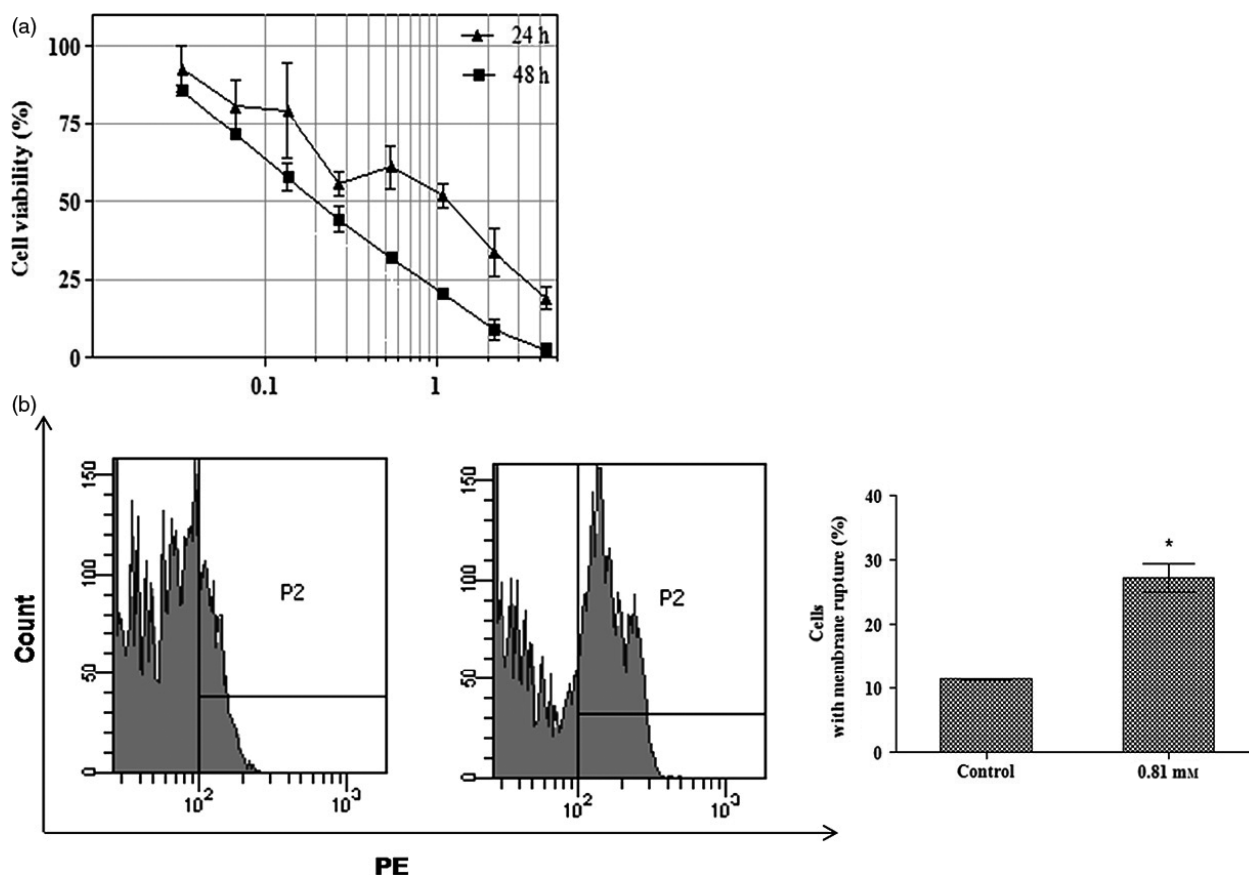


Figure 3 (a) Cytotoxic effects of LQFM030 on EAT cells after 24 and 48 h of treatment (0.033–4.32 mM). Cell viability was examined with trypan blue exclusion method and expressed as a percentage of the control. Experiments were performed in sextuplicate. Each bar presents means \pm SD of three independent experiments. The IC₅₀ values were 0.81 and 0.10 mM, respectively. (b) Effects of LQFM030 on plasma membrane integrity. EAT cells were treated for 24 h with 0.81 mM LQFM030 and analysed on a flow cytometer. Histograms displaying PE fluorescence (x-axis) versus counts (y-axis) have been shown in logarithmic fluorescence intensity. The bar presents mean \pm SD of two independent experiments (* $P < 0.05$ compared with control).

cells (Annexin V +/PI +; $P < 0.05$). Furthermore, the number of necrotic or secondary necrotic cells (Annexin V –/PI +) also increased to $19.65 \pm 0.49\%$ ($P < 0.05$). These data suggest that EAT cell death mechanism triggered by LQFM030 (2) is apoptosis.

Analysis of DNA fragmentation was determined after the treatment of EAT cells with LQFM030 (2). As observed in Figure 6d–f, treatment with 810 μ M LQFM030 (2) for 24 h increased DNA fragmentation by $38.1 \pm 9.6\%$ compared with the control cells ($2.1 \pm 0.07\%$, $P < 0.05$).

LQFM030 (2) modulated p21, p27, p53 mRNA and protein levels in EAT cells

Because the obtained data suggest that LQFM030 (2) triggers cell cycle arrest and apoptosis, the mechanisms involved in these processes were explored. It is well

known that p53 activation promotes cycle arrest via p21WAF1/CIP1, which is a potent cyclin-dependent kinase (CDK) inhibitor that can effectively block the cell cycle progression in G1 and G2 phases. In addition, p27 is another CDK inhibitor also promoting cell cycle arrest.^[35] Thus, the role of these proteins was evaluated in EAT cells after LQFM030 (2) treatment (Figure 7a–i). Our results showed an increase in p21 ($81.25 \pm 2.89\%$), p27 ($68.20 \pm 3.67\%$) and p53 ($33.80 \pm 5.76\%$) protein levels in the treated EAT cells compared with the control ($34.10 \pm 3.81\%$, $26.80 \pm 1.55\%$ and $12.03 \pm 2.32\%$, respectively; $P < 0.05$). Similar to protein level, p21 mRNA also increased; however, p53 mRNA levels did not show significant changes, suggesting that the increase in p53 protein reflects its decreased degradation rather than the induction of p53 mRNA transcription level (Figure 7j–l).

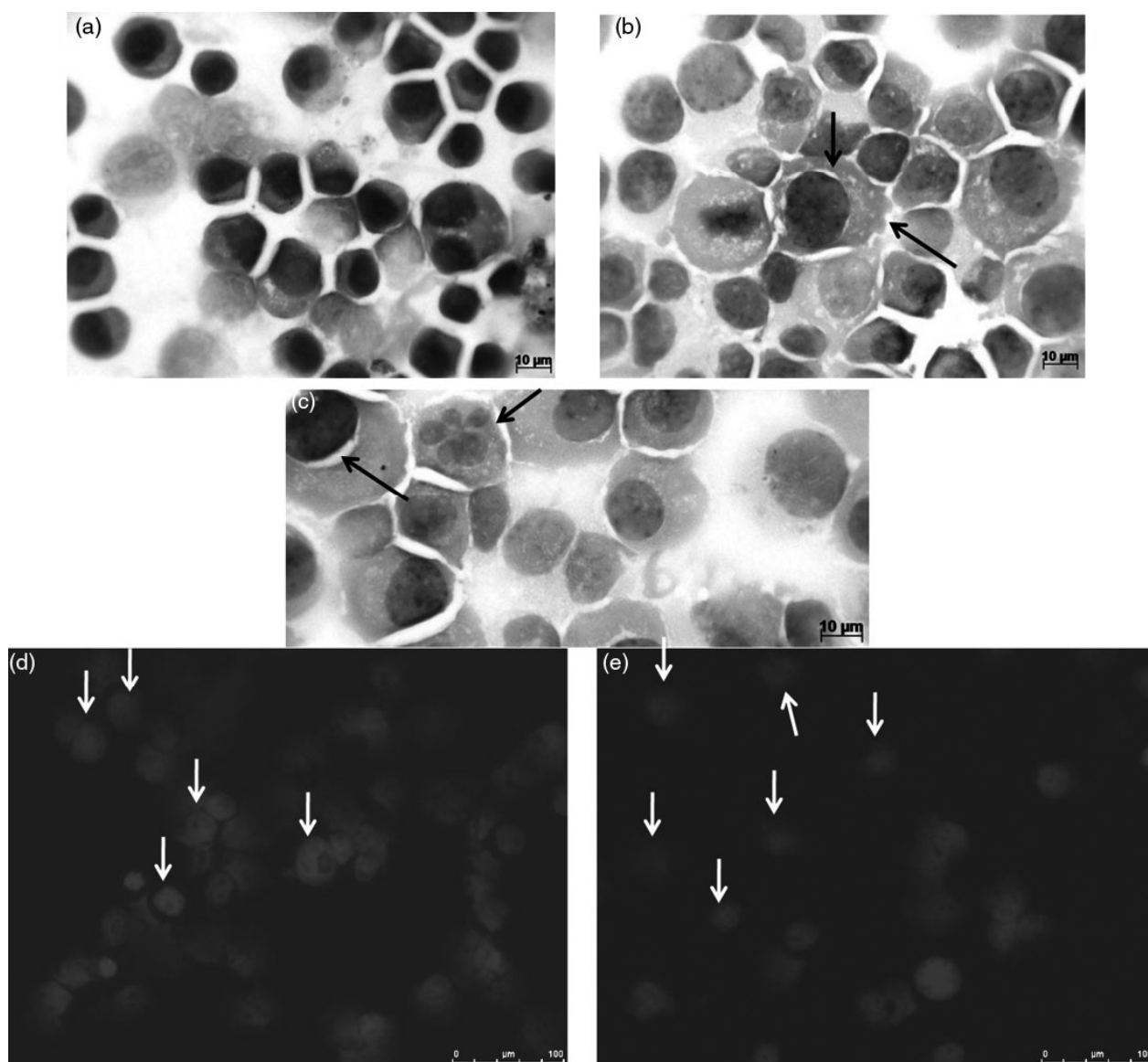


Figure 4 Apoptotic morphology of EAT cells upon LQFM030 treatment. The cells were treated with 0.81 mM LQFM030 for 24 h and stained with HE. Images were taken using a 100× objective with the AxioVs40 software. (a) Control cells showing nuclei with dispersed chromatin and organized plasma membrane. (b) LQFM030-treated cells presenting membrane blebbing and vacuolization (arrows) (c) Treated cells presenting nuclear fragmentation and vacuolization (arrows). Changes in the nuclear morphology of EAT cells. Nuclear staining was performed with Hoechst 33342. Images were taken using a 20× objective with LAS-AF software. (d) Control cells. (e) LQFM030-treated cells presenting chromatin condensation, low fluorescence and shrinking nuclei.

LQFM030 (2) treatment changes MDM2 mRNA and protein levels in EAT cells

Once the LQFM030 (2) increased p53 protein expression, the next step was to analyse the mRNA and protein levels of MDM2. A Western blot analysis of the p53 inhibitor protein MDM2 showed that MDM2 decreased after 24 h

of treatment with LQFM030 (2) (0.06 ± 0.05), with a significant reduction in the band density in relation to the control cells (0.37 ± 0.13) (Figure 8a,b). Strikingly, unlike protein analysis that revealed MDM2 protein decreases after LQFM030 (2) treatment in EAT cells, the MDM2 mRNA levels were found to be increased (Figure 8c).

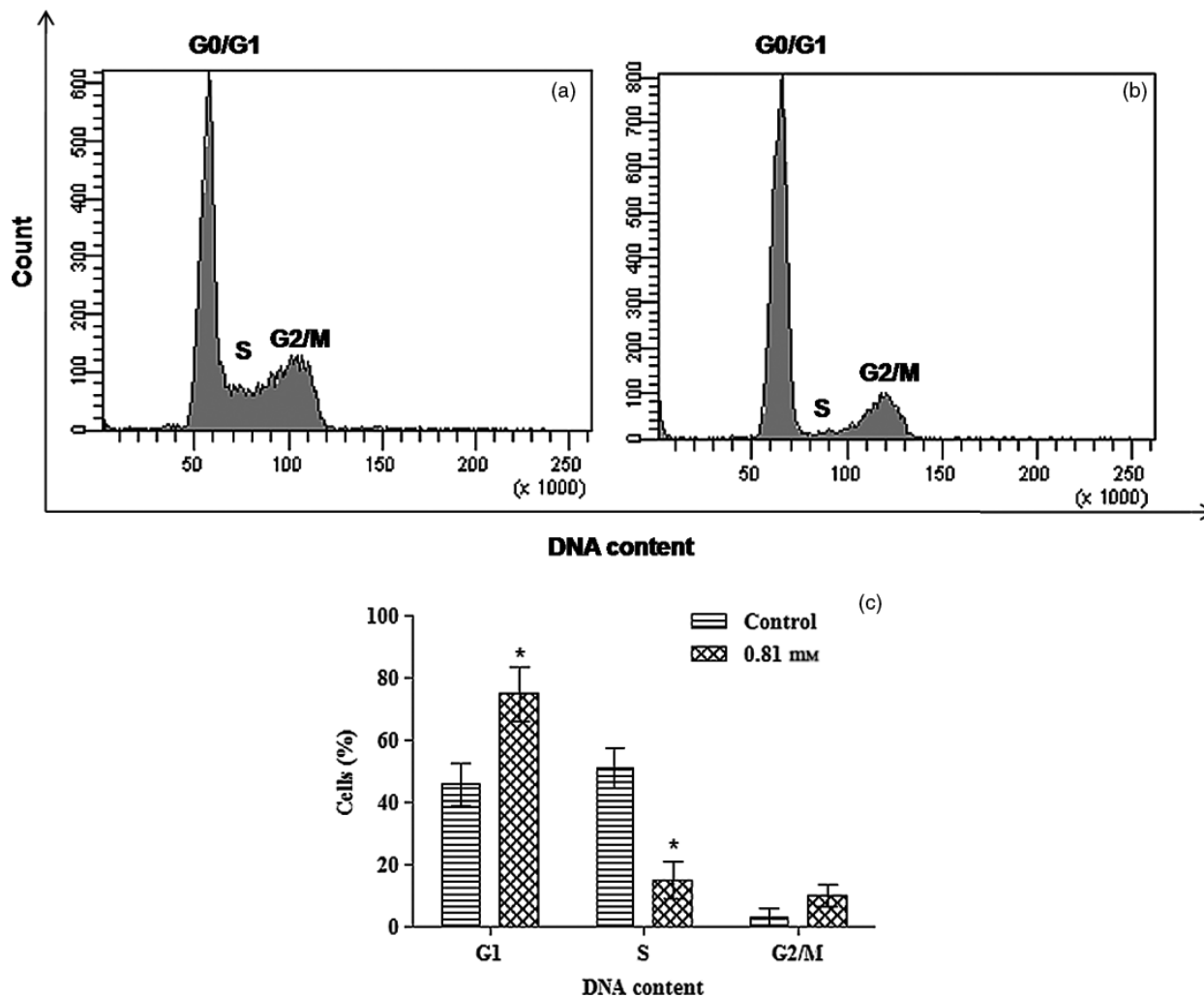


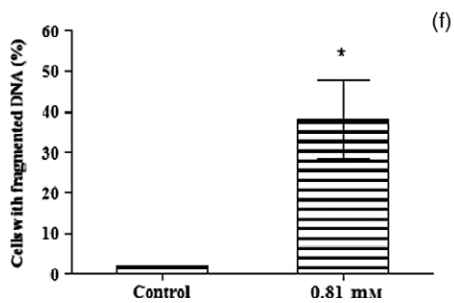
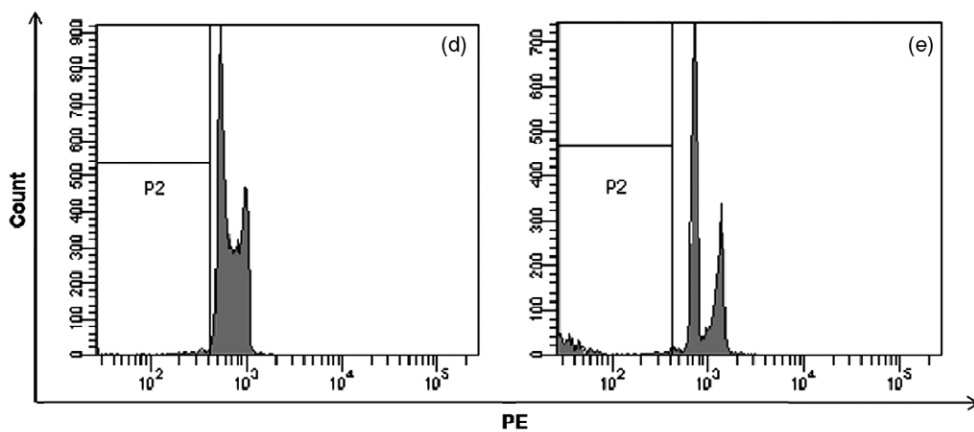
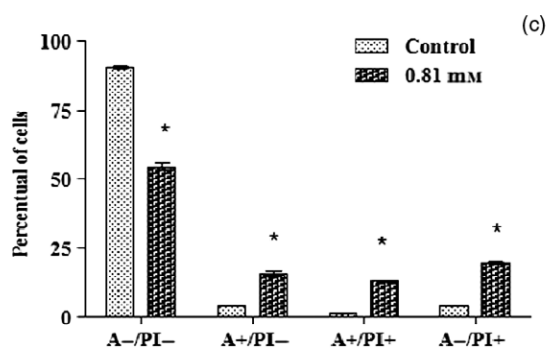
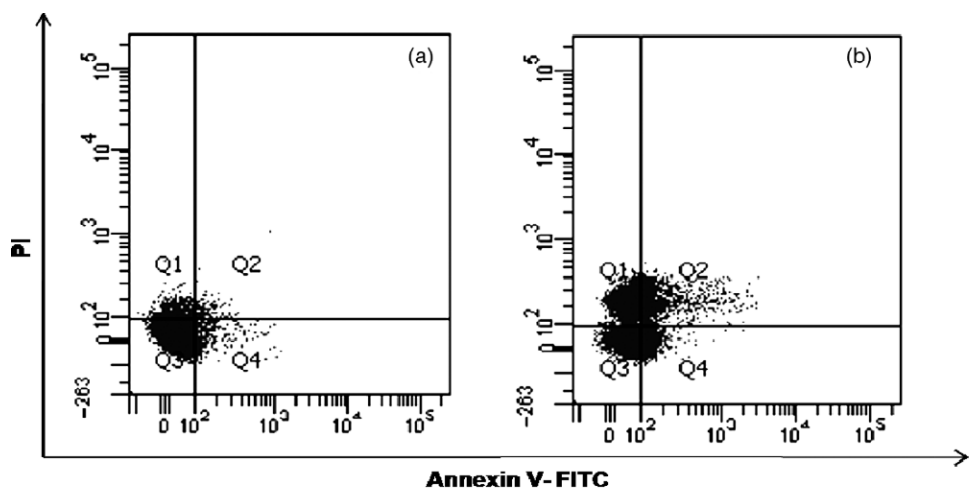
Figure 5 Analysis of the effects of LQFM030 on EAT cell cycle. For the determination of cell cycle-phase distribution, EAT cells were permeabilized and nuclear DNA was labelled with propidium iodide (PI). The analysis was carried out by flow cytometry. The histograms show (a) untreated cells, (b) cells treated with 0.81 mM LQFM030 for 24 h, (c) percentage of EAT cells in G1, S and G2 phases before and after LQFM030 treatment. Each bar presents mean \pm SD of three independent experiments (* $P < 0.05$ compared with control).

LQFM030 (2) induced caspase-mediated apoptosis in EAT cells

To further investigate the death mechanisms elicited by this compound, the activity of caspases-3/7, -8 and -9 was measured. We observed a 2.8-fold increase in

caspase-8, 3.7-fold increase in caspase-9 and 4-fold increase in caspase-3 compared with the control cells ($P < 0.05$) (Figure 9a–i). Similar to protein, caspase-9 mRNA presented high levels, while caspase-8 mRNA slightly increased (Figure 9j–l). In contrast, caspase 3 mRNA levels decreased (Figure 9m). Although apparently

Figure 6 Flow cytometry analysis of phosphatidylserine externalization in LQFM030-treated EAT cells. Cells were stained with Annexin V-FITC and PI. (a) Untreated cells and (b) cells treated with 0.81 mM LQFM030 for 24 h. Left inferior squares (Annexin V $-$ /PI $-$) = % viable cells. Right inferior squares (Annexin V $+$ /PI $-$) = % early apoptotic cells. Left superior squares (Annexin V $+$ /PI $+$) = % late apoptotic cells. Right superior squares (Annexin V $-$ /PI $+$) = % necrotic cells. (c) Comparison of fluorescence intensity of Annexin V-FITC and PI between untreated and LQFM030-treated cells. The bar presents mean \pm SD of two independent experiments (* $P < 0.05$ compared with control). (d–f) Percentage of DNA fragmentation in LQFM030-treated EAT cells. EAT cells were treated for 24 h with 0.81 mM LQFM030 and analysed on a flow cytometer. Histograms displaying PE fluorescence (x-axis) versus counts (y-axis) have been shown in logarithmic fluorescence intensity. (d) Untreated cells, (e) cells treated with 0.81 mM LQFM030 for 24 h, (f) comparison of fluorescence intensity of PI between untreated and LQFM030-treated cells. The bar presents mean \pm SD of two independent experiments (* $P < 0.05$ compared with control).



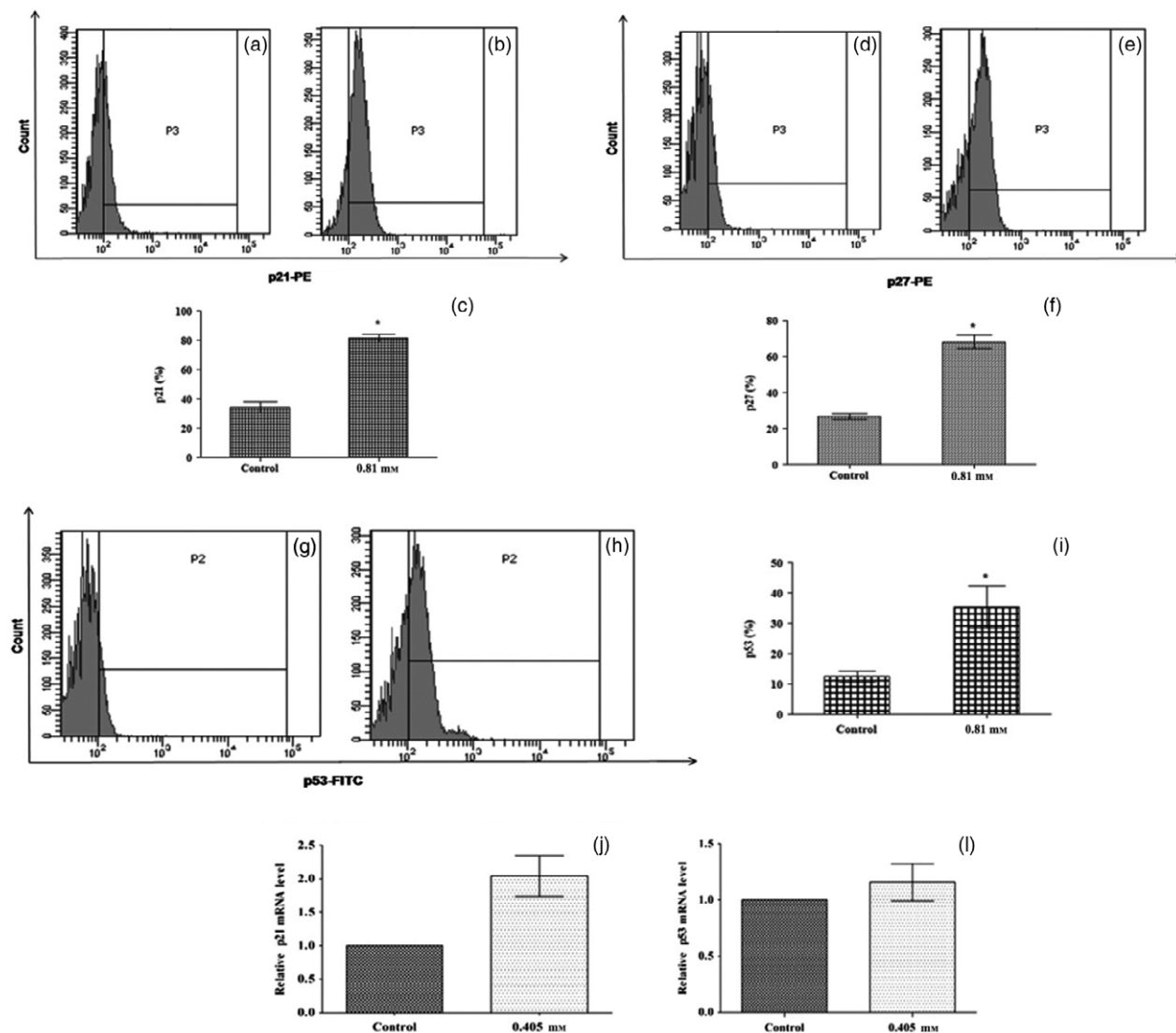


Figure 7 Effect of LQFM030 on the expression of p21, p27 and p53. EAT cells were treated for 24 h with 0.81 mM LQFM030 and analysed on a flowcytometer. Histograms displaying PE/FITC fluorescence (x-axis) versus counts (y-axis) have been shown in logarithmic fluorescence intensity. (a,d,g) Untreated cells. (b,e,h) Cells treated with 0.81 mM LQFM030 for 24 h. (c,f,i) Comparison of fluorescence intensity of PE/FITC between untreated and LQFM030-treated cells. The bar presents mean \pm SD of two independent experiments (* $P < 0.05$ compared with control). (j,l) Real-time PCR analysis of p21 and p53 mRNA after exposure to 0.405 mM LQFM030 for 24 h. The normalized gene was PGK1. The data were obtained from two independent experiments, repeated three times, and standard error bars (\pm SD) represent intra-experimental error.

counterintuitive, this result suggests that the effector caspase activated by LQFM030 (2) treatment was caspase-7, instead of caspase-3.

Discussion

Considering the crucial role of p53 in tumour suppression, the reactivation of the p53 function by disrupting the p53–MDM2 interaction using inhibitors agents is now recognized as a promising strategy for anticancer drug design. Many series of small-compound inhibitors have been

described to date, including benzodiazepinediones, nutlins, spiro-oxindoles, quinolinols, isoindolinones, sulfonamides, chalcones, terphenyls and piperazine-4-phenyl derivatives, many of which show relatively weak bioactivity. Within this context, only the nutlins, spiro-oxindoles and benzodiazepinediones are considered to be particularly valuable.^[3,9,36]

Several studies revealed the potential of nutlins in inhibiting the p53–MDM2 interaction, promoting cell cycle arrest and triggering apoptosis in different cancer cell lines.^[6,9,37–44]

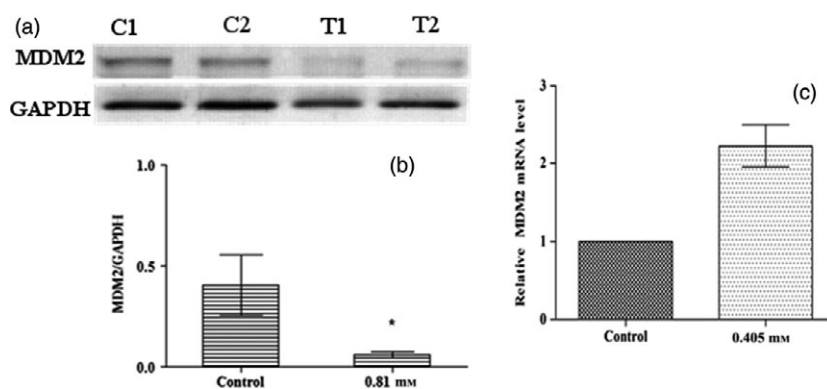


Figure 8 Effect of LQFM030 on the expression of MDM2. (a) Western blot analysis after the treatment of EAT cells for 24 h with 0.81 mM LQFM030. Blot of two independent experiments (C1 and T1 – control and treated cells, respectively, of experiment 1; C2 and T2 – control and treated cells, respectively, of experiment 2). GAPDH is shown as a loading control. (b) Band density of untreated and LQFM030-treated cells calculated as the ratio of GAPDH expressed in the same sample. The bar presents mean \pm SD of two independent experiments (* $P < 0.05$ compared with control). (c) Real-time PCR analysis of MDM2 mRNA after exposure to 0.405 mM LQFM030 for 24 h. The normalized gene was PGK1. The data were obtained from two independent experiments, repeated three times, and standard error bars (\pm SD) represent intra-experimental error.

In this work, we report the synthesis, characterization and biological properties of LQFM030 (**2**). This compound was derived from molecular simplification of the lead compound nutlin 1 (**1**), where subunits A, B and C of the nutlin-1 (**1**) were preserved in LQFM030 (**2**) and the chiral centres were removed, making the synthesis easier and cheaper. The data showed that LQFM030 (**2**) can interfere on the p53–MDM2 interaction that effectively activates the p53 pathway and induces cell cycle arrest or apoptosis in wild-type p53 EAT cells. The identified cell growth inhibition was concentration dependent with the loss of plasma membrane integrity and DNA fragmentation.

P53 pathway activation by nutlin 1 occurs due to the decreased degradation of p53 rather than the elevated expression of the p53 gene, once p53 transcript level was not affected by nutlin treatment.^[6] Similar results were obtained with LQFM030 (**2**) compound; an increased amount of p53 was detected by cytometry, but p53 transcript level was not altered by LQFM030 (**2**). In addition, p21 and p27 protein and mRNA increased after the treatment with LQFM030 (**2**).

Other small-molecule inhibitors of p53–MDM2 interactions, such as nutlins, RG7112 (nutlin derivative), RG7388 and M-219, also present a similar pattern in wild-type p53 cells, as expected.^[6,37,45,46] Indeed, RG-7112, another nutlin derivative, advanced into clinical development.^[47] Strikingly, RITA, another inhibitor of p53–MDM2 interactions in wt-p53 cells, does not depend on p21 activity in growth suppression. One probable explanation is that RITA disrupts p53–MDM2 interaction; RITA binds to p53, not to MDM2 protein.^[48] It is essential to know that p53–MDM2 disruption can trigger different cell death mechanisms,

because the relative impact of apoptotic activity and other activity of p53 could either enhance or prevent the therapeutic response.^[48]

In relation to MDM2, LQFM030 (**2**) increased MDM2 mRNA, but reduced MDM2 protein, probably associated with an increase in its degradation. In most studies, nutlin compounds promote MDM2 increase in protein and mRNA levels in almost all wild-type p53 tumour cells.^[6,41,43–45] Furthermore, the pharmacological strategy based on nutlin-3a tends to have transient effects and is counterbalanced by the strong feedback loop regulating the reciprocal interactions between MDM2 and p53.^[11] However, the nutlin 3-s treatment of B-cell chronic lymphocytic leukaemia (B-CLL), in which low level expression of p53 transcripts was found, does not upregulate MDM2 despite the progressive stabilization and the accumulation of p53 and its targets.^[46] The variability in MDM2 expression in tumour cell responses after nutlin-3 treatment indicates that under some circumstances and tumour cell types, this compound can induce the different cell death mechanisms. Concerning specifically MDM2 protein and mRNA expression, our results are similar to those obtained with MI-219, a spiro-oxindole MDM2 antagonist, which promoted an increase in MDM2 transcripts, but downregulated the protein level. The authors suggested that MI-219 post-translational process regulates HDM2 protein by inducing autoubiquitination and the degradation of itself.^[46,49] This could be, at least in part, an explanation for the decrease in MDM2 protein after LQFM030 (**2**) treatment. Moreover, nutlin-3 stabilizes MDM2's conformation and protects MDM2 from degradation.^[46] Our results *in vitro* are in accordance with the *in-silico* study.

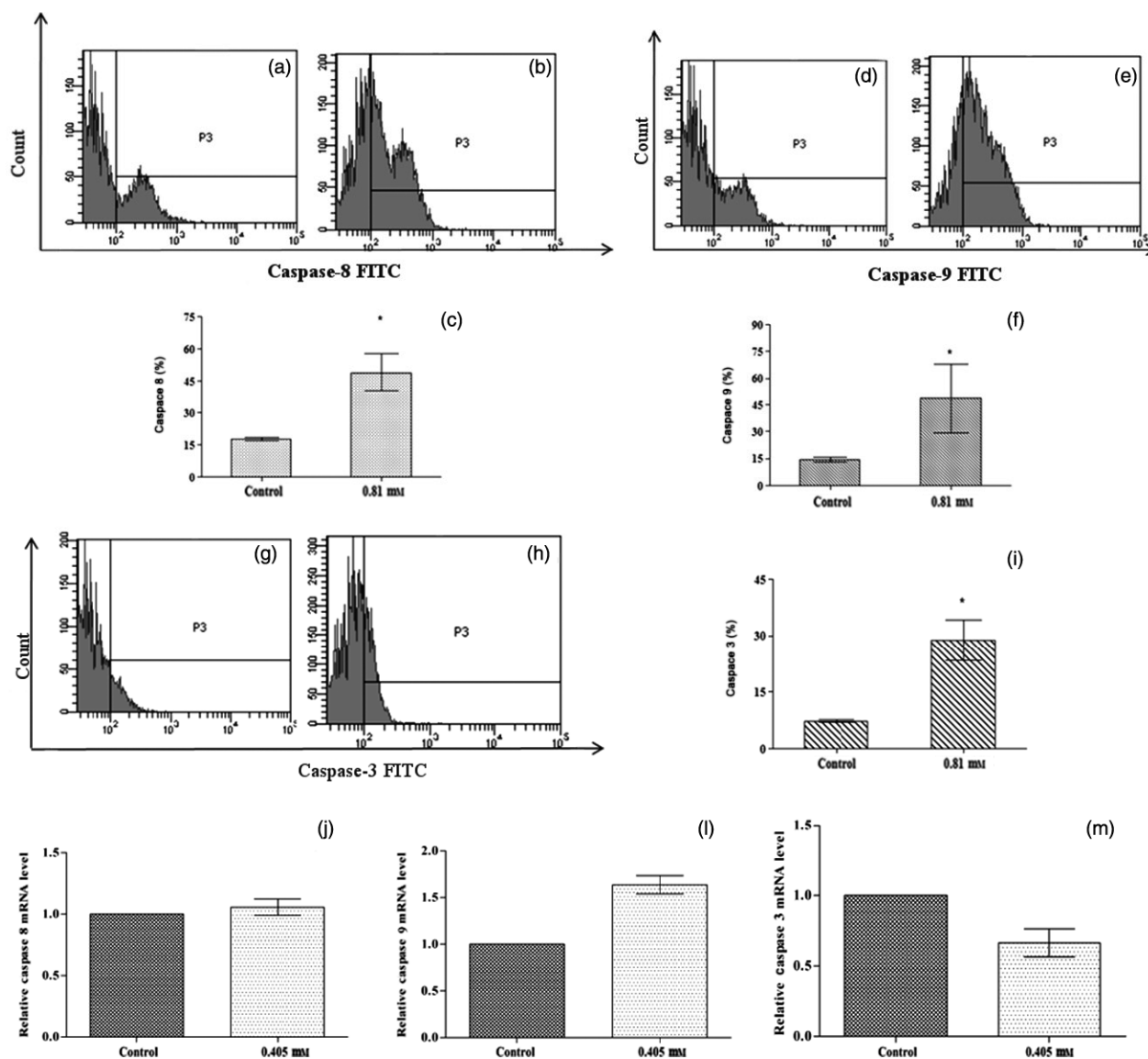


Figure 9 Effect of LQFM030 on the activity of caspase-8, -9 and -3/7. (a,d,g) Untreated cells. (b,e,h) Cells treated with 0.81 mM LQFM030 for 24 h. (c,i,f) Comparison of fluorescence intensity of FITC between untreated and LQFM030-treated cells. Each bar presents mean \pm SD of two independent experiments (* $P < 0.05$ compared with control). (j,l,m) Real-time PCR analysis of caspases-8, -9 and -3 mRNA after exposure to 0.405 mM LQFM030 for 24 h. The normalized gene was PGK1. The data were obtained from two independent experiments, repeated three times, and standard error bars (\pm SD) represent intra-experimental error.

Even though at least *in vitro*, caspase activation is not a strict requirement for multiple cases of apoptosis,^[34] the above findings prompted us to further investigate whether caspases would play a role in cell death after LQFM030 (2) treatment, because it is well established that caspase activation is involved in the nutlin-induced apoptotic programme.^[6,46,50,51] Our results revealed that similar to nutlins, mRNA level and activity of all caspases analysed showed an increased activity after the treatment. These

results suggest the activation of both intrinsic and extrinsic apoptotic pathways.

Previous studies revealed that p53 has a direct apoptogenic role in the mitochondria in response to multiple death stimuli. A rapid p53 translocation to mitochondria, after death stimuli, triggers a first wave of apoptosis that is transcription independent and may precede a second slower wave that is transcription dependent.^[52,53] Later studies showed that the direct mitochondrial programme is

a major mechanism in nutlin-induced p53-mediated apoptosis in tumour cells; apoptosis occurred through the caspase activation.^[53] p53 translocation to the mitochondria promotes its interaction with Bcl2 family members and induces mitochondrial outer membrane permeabilization (MOMP). The characteristic of caspase-dependent intrinsic apoptosis relies on MOMP induction with the subsequent activation of caspase-9 initiator and caspase-3 effector.^[34] This seems to be the most common mechanism of intrinsic apoptosis because caspase-3 is the best well-characterized effector caspase.^[54,55] Our results with LQFM030 (2) showed that both caspase-9 mRNA and protein increased, leading to the effector caspase-3/7 activation. Nevertheless, despite the increase in effector caspase-3/7 activity, the caspase-3 mRNA decreased after the treatment. This result suggests that the effector caspase activated by LQFM030 (2) is caspase-7. Interestingly, Devarajan *et al.*^[57] described that approximately 75% of the breast tumour cells analysed in their study revealed the lack of caspase-3 transcripts and caspase-3 protein expression, while the remaining samples showed substantial decreases in caspase-3 expression. Because EAT cells are derived from murine breast carcinoma, our data are in agreement with these results. Furthermore, studies conducted in *CASP-3*-deficient MCF-7 cells revealed that caspase-7 is indeed responsible for the proteolysis during the demolition phase of apoptosis.^[57] Regardless of whether caspase-8 mRNA did not alter after the LQFM030 (2) treatment, its activity increased significantly, indicating that our compound also induces extrinsic pathway, similar to nutlins.^[51,58] Apparently, the extrinsic and intrinsic apoptotic pathways show a key role in response to p53 activation.^[3] In sum, the in-vitro results were in agreement with in-silico results.

The current paradigm of anticancer drug therapy is the development compounds with nanomolar in-vitro potency, showing that they would be efficacious and safer based on

the assumption that they can be used at lower doses ('the nanomolar rule'). However, critical parameters such as the balance between efficacy and toxicity are ignored, rejecting the efficacious compounds or selecting the ineffective or toxic compounds. Moreover, there are efficacious anticancer agents lacking the nanomolar potency.^[59,60] According to Secchiero *et al.*,^[1] it will be unlikely that nutlin-3 will be used as a monotherapy, but combined with innovative drugs, such as TRAIL or bortezomib, might be an effective approach in cancer therapy. In a similar way, LQFM030 (2) could be combined with other therapeutic agents to increase the treatment efficacy. Another approach would be LQFM030 (2) optimization, which is under way.

Conclusion

Our results suggested that a simplified analogue of nutlin-1, LQFM030 (2), could have an inhibitory effect on the p53–MDM2 interaction, reactivating p53 and its main functions, cell cycle arrest and apoptosis. These results suggest that the small-molecule p53 activator LQFM030 (2) could be of value in the development of a novel cancer therapeutic agent.

Declarations

Funding

This study was supported by Fundação de Apoio à Pesquisa (FUNAPE)-UFG, Goiânia-GO, Conselho Nacional de Desenvolvimento Científico e Tecnológico (CNPq), Financiadora de Estudo e Projetos (FINEP), Coordenação de Aperfeiçoamento de Pessoal de Nível Superior (CAPES) and Fundação de Apoio a Pesquisa do Estado de Goiás (FAPEG).

References

1. Secchiero P *et al.* Recent advances in the therapeutic perspectives of nutlin-3. *Curr Pharm Des* 2011; 17: 569–577.
2. Shen H, Maki CG. Pharmacologic activation of p53 by small-molecule MDM2 antagonists. *Curr Pharm Des* 2011; 17: 560–568.
3. Khoo KH *et al.* Drugging the p53 pathway: understanding the route to clinical efficacy. *Nat Rev Drug Discov* 2014; 13: 217–236. Erratum in: *Nat Rev Drug Discov* 2014; 13: 314.
4. Chattopadhyay S *et al.* Protein A-activated macrophages induce apoptosis in Ehrlich's ascites carcinoma through a nitric oxide-dependent pathway. *Apoptosis* 2002; 7: 49–57.
5. Janouskova H *et al.* Activation of p53 pathway by Nutlin-3a inhibits the expression of the therapeutic target $\alpha 5$ integrin in colon cancer cells. *Cancer Lett* 2013; 336: 307–318.
6. Vassilev LT *et al.* In vivo activation of the p53 pathway by small-molecule antagonists of MDM2. *Science* 2004; 303: 844–848.
7. Mir R *et al.* Mdm2 antagonists induce apoptosis and synergize with cisplatin overcoming chemoresistance in TP53 wild-type ovarian cancer cells. *Int J Cancer* 2013; 132: 1525–1536.
8. Van Maerken T *et al.* Pharmacologic activation of wild-type p53 by nutlin therapy in childhood cancer. *Cancer Lett* 2014; 344: 157–165.
9. Vassilev LT. MDM2 inhibitors for cancer therapy. *Trends Mol Med* 2007; 13: 23–31.
10. Klein G. Some recent studies on the production and growth characteristics

- of ascites tumors, a review. *Z Krebsforsch* 1956; 61: 99–119.
11. Hartveit FM. Experimental studies on the immune response to Ehrlich's ascites carcinoma. 1964. With the due permission of the senate of the University of Bergen to be publicly discussed on the 13th May for the degree of Doctor medicine.
 12. Tokalov SV, Iagunov AS. Radiation-induced cell cycle arrests in Ehrlich ascites carcinoma cells in vivo. *Radiat Environ Biophys* 2011; 50: 265–270.
 13. Finar IL, Godfrey KE. The preparation and properties of some derivatives of 1-phenylpyrazole. *J Chem Soc* 1954; 2293–2298.
 14. de Oliveira CHA et al. Chemoselective and regioselective formylation of 1-phenyl-1H-pyrazoles through the Duff reaction. *Synth Commun* 2013; 43: 1633–1639.
 15. Anil B et al. The structure of an MDM2-Nutlin-3a complex solved by the use of a validated MDM2 surface-entropy reduction mutant. *Acta Crystallogr* 2013; 69: 1358–1366.
 16. Hanwell MD et al. Avogadro: an advanced semantic chemical editor, visualization, and analysis platform. *J Cheminform* 2012; 4: 17.
 17. Breneman CM, Wiberg KB. Determining atom-centered monopoles from molecular electrostatic potentials: the need for high sampling density in formamide conformational analysis. *J Comput Chem* 1990; 11: 361–373.
 18. Schmidt MW et al. General atomic and molecular electronic structure system. *Comput Chem* 1993; 14: 1347–1363.
 19. Gordon MS, Schmidt MW. Advances in electronic structure theory: GAMESS a decade later. In: Dykstra CE, Frenking G, Kim KS, Scuseria GE, eds. *Theory and Applications of Computational Chemistry: The First Forty Years*. Elsevier: Amsterdam, 2005: 1167–1189.
 20. Sanner MF. Python: a programming language for software integration and development. *J Mol Graph Model* 1999; 17: 57–61.
 21. Morris GM et al. Autodock4 and AutoDockTools4: automated docking with selective receptor flexibility. *J Comput Chem* 2009; 16: 2785–2791.
 22. de Magalhães CS et al. A dynamic niching genetic algorithm strategy for docking highly flexible ligands. *Inf Sci* 2014; 289: 206–224.
 23. Custódio FL et al. A multiple minima genetic algorithm for protein structure prediction. *Appl Soft Comput* 2014; 15: 88–99.
 24. Morris GM et al. Automated docking using a Lamarckian genetic algorithm and empirical binding free energy function. *J Comput Chem* 1998; 19: 1639–1662.
 25. Laskowski RA, Swindells MB. LigPlot+: multiple ligand-protein interaction diagrams for drug discovery. *J Chem Inf Model* 2011; 51: 2778–2786.
 26. Mota MF et al. Investigation of Ehrlich ascites tumor cells death mechanisms induced by *Synadenium umbellatum* Pax. *J Ethnopharmacol* 2012; 139: 319–329.
 27. Boley SE et al. p53 heterozygosity alters the mRNA expression of p53 target genes in the bone marrow in response to inhaled benzene. *Toxicol Sci* 2002; 66: 209–215.
 28. Yang C et al. Transcriptional activation of caspase-6 and -7 genes by cisplatin-induced p53 and its functional significance in cisplatin nephrotoxicity. *Cell Death Differ* 2008; 15: 530–544.
 29. Breuss M et al. Mutations in the β -tubulin gene TUBB5 cause microcephaly with structural brain abnormalities. *Cell Rep* 2012; 2: 1554–1562.
 30. Livak KJ, Schmittgen TD. Analysis of relative gene expression data using real-time quantitative PCR and the 2^{- $\Delta\Delta$ C_T} method. *Methods* 2001; 25: 402–408.
 31. Fry DC et al. NMR structure of a complex between MDM2 and a small molecule inhibitor. *J Biomol NMR* 2004; 30: 163–173.
 32. Klein C, Vassilev LT. Targeting the p53-MDM2 interaction to treat cancer. *Br J Cancer* 2004; 91: 1415–1419.
 33. Qu X et al. Autophagy gene-dependent clearance of apoptotic cells during embryonic development. *Cell* 2007; 128: 931–946.
 34. Galluzzi L et al. Molecular definitions of cell death subroutines: recommendations of the Nomenclature Committee on Cell Death 2012. *Cell Death Differ* 2012; 19: 107–120.
 35. Foijer F, te Riele H. Check, double check: the G2 barrier to cancer. *Cell Cycle* 2006; 5: 831–836.
 36. Guo Z et al. Structure-activity relationship and antitumor activity of thio-benzodiazepines as p53-MDM2 protein-protein interaction inhibitors. *Eur J Med Chem* 2012; 56: 10–16.
 37. Tovar C et al. Small-molecule MDM2 antagonists reveal aberrant p53 signaling in cancer: implications for therapy. *Proc Natl Acad Sci USA* 2006; 103: 1888–1893.
 38. Cheok CF et al. Cyclin-dependent kinase inhibitors sensitize tumor cells to nutlin-induced apoptosis: a potent drug combination. *Mol Cancer Res* 2007; 5: 133–145.
 39. Secchiero P et al. The MDM2 inhibitor nutlins as an innovative therapeutic tool for the treatment of haematological malignancies. *Curr Pharm Des* 2008; 14: 2100–2110.
 40. Pishas KI et al. Nutlin-3a is a potential therapeutic for ewing sarcoma. *Clin Cancer Res* 2011; 17: 494–504.
 41. Miyachi M et al. Restoration of p53 Pathway by nutlin-3 induces cell cycle arrest and apoptosis in human rhabdomyosarcoma cells. *Clin Cancer Res* 2009; 15: 4077–4084.
 42. Ghassemifar S, Mendrysa SM. MDM2 antagonism by nutlin-3 induces death in human medulloblastoma cells. *Neurosci Lett* 2012; 513: 106–110.
 43. Künkele A et al. Pharmacological activation of the p53 pathway by nutlin-3 exerts anti-tumoral effects in medulloblastomas. *Neuro Oncol* 2012; 14: 859–869.
 44. Ye F et al. Nutlin-3 induces apoptosis, disrupts viral latency and inhibits expression of angiopoietin-2 in Kaposi sarcoma tumor cells. *Cell Cycle* 2012; 11: 1393–1399.
 45. Park EJ et al. Nutlin-3, a small-molecule MDM2 inhibitor, sensitizes Caki

- cells to TRAIL-induced apoptosis through p53-mediated PUMA upregulation and ROS-mediated DR5 upregulation. *Anticancer Drugs* 2013; 24: 260–269.
46. Ding Q *et al.* Discovery of RG7388, a potent and selective p53-MDM2 inhibitor in clinical development. *J Med Chem* 2013; 56: 5979–5983.
47. Sosin AM *et al.* HDM2 antagonist MI-219 (spiro-oxindole), but not Nutlin-3 (cis-imidazoline), regulates p53 through enhanced HDM2 autoubiquitination and degradation in human malignant B-cell lymphomas. *J Hematol Oncol* 2012; 5: 57.
48. Zhao Y *et al.* Small Molecule inhibitors of MDM2-p53 and MDMX-p53 interaction as new cancer therapeutics. *BioDiscovery* 2013; 8: 4.
49. Enge M *et al.* MDM2-dependent downregulation of p21 and hnRNP K provides a switch between apoptosis and growth arrest induced by pharmacologically activated p53. *Cancer Cell* 2009; 15: 171–183.
50. Shangary S *et al.* Temporal activation of p53 by a specific MDM2 inhibitor is selectively toxic to tumors and leads to complete tumor growth inhibition. *Proc Natl Acad Sci USA* 2008; 105: 3933–3938.
51. Tabe Y *et al.* MDM2 antagonist nutlin-3 displays antiproliferative and proapoptotic activity in mantle cell lymphoma. *Clin Cancer Res* 2009; 15: 933–942.
52. Kojima K *et al.* MDM2 antagonists induce p53-dependent apoptosis in AML: implications for leukemia therapy. *Blood* 2005; 106: 3150–3319.
53. Mihara M *et al.* p53 has a direct apoptogenic role at the mitochondria. *Mol Cell* 2003; 11: 577–590.
54. Erster S *et al.* *In vivo* mitochondrial p53 translocation triggers a rapid first wave of cell death in response to DNA damage that can precede p53 target gene activation. *Mol Cell Biol* 2004; 24: 6728–6741.
55. Vaseva AV *et al.* The transcription-independent mitochondrial p53 program is a major contributor to nutlin-induced apoptosis in tumor cells. *Cell Cycle* 2009; 8: 1711–1719.
56. Parrish AB *et al.* Cellular mechanisms controlling caspase activation and function. *Cold Spring Harb Perspect Biol* 2013; 5: 1–24.
57. Devarajan E *et al.* Down-regulation of caspase 3 in breast cancer: a possible mechanism for chemoresistance. *Oncogene* 2002; 21: 8843–8851.
58. Walsh JG *et al.* Executioner caspase-3 and caspase-7 are functionally distinct proteases. *Proc Natl Acad Sci USA* 2008; 105: 12815–12819.
59. Saha MN *et al.* Molecular mechanisms of nutlin-induced apoptosis in multiple myeloma: evidence for p53-transcription-dependent and -independent pathways. *Cancer Biol Ther* 2010; 10: 567–578.
60. Wong CC *et al.* Preclinical predictors of anticancer drug efficacy: critical assessment with emphasis on whether nanomolar potency should be required of candidate agents. *J Pharmacol Exp Ther* 2012; 341: 572–578.